Original scientific paper

MECHANICALLY PRESSED POLYMER-MATRIX COMPOSITES WITH 3D STRUCTURED FILLER NETWORKS FOR ELECTROMAGNETIC INTERFERENCE SHIELDING APPLICATION

Chunghyun Choi[1], Nadeem Qaiser[2], Byungil Hwang[3]

[1]Department of Intelligent Semiconductor Engineering, Chung-Ang University, South Korea
[2]Material Science and Engineering, Physical Science and Engineering Division, King Abdullah University of Science and Technology (KAUST), Saudi Arabia
[3]School of Integrative Engineering, Chung-Ang University, South Korea

ORCID iDs: Chunghyun Choi	https://orcid.org/0009-0001-7634-9933
Nadeem Qaiser	https://orcid.org/0000-0001-7417-9857
Byungil Hwang	https://orcid.org/0000-0001-9270-9014

Abstract. *The increasing demand for miniaturization, high-power density, and high-frequency electronic devices highlights the importance of polymer composites with high electromagnetic interference (EMI) shielding. These composites are crucial to maintaining devices, reducing communication errors, and protecting human health. In this study, we developed a mechanically pressed composite of polystyrene, MXene, and boron nitride nanosheets (BNNSs) with a 3D structured filler network through electrostatic interactions and the hot-pressing technique. Constructing a 3D filler network within the composite led to a significant EMI shielding effect, particularly in the low-frequency range. Furthermore, it was observed that the BNNSs-coated sample contributed to superior EMI shielding effectiveness compared to the non-coated sample. This suggests that BNNSs improve the EMI shielding effectiveness by providing additional interfaces within the composite and help prevent the degradation of MXene. We expect our study to provide valuable insights into the development of 3D structured filler networks within composites while contributing to improvements in thermal conductivity and EMI shielding performance.*

Key words: *Polymer-matrix composites, 3D structured hybrid fillers network, Electromagnetic interference shielding, Electrical insulation, 2D materials, MXene, Boron nitride nanosheets.*

1. INTRODUCTION

Owing to the development of 5G wireless communication, coupled with high-frequency and high-power density devices, advanced electronic devices induce electromagnetic waves, which can adversely impact human health and the environment [1-6]. Furthermore, due to the interference of the generated electromagnetic waves, electromagnetic interference (EMI) influences the stability and accuracy of devices. This poses a significant issue, especially in areas where devices are densely packed or in high-precision equipment and sensitive electronic systems. For example, malfunctions due to EMI in medical equipment, aircraft, and military systems can lead to severe consequences [7-10].

Polymers are widely used as matrices to fabricate functional composites due to their advantages such as their lightweight nature, low cost, and processability. However, pure polymers have electrically insulating properties. Theoretically, to prepare composites with outstanding EMI shielding effectiveness (EMI SE), high electrically conductive materials are required. Therefore, fillers are introduced into polymer matrices to attain high electrical conductivity. Selecting an appropriate filler is a crucial factor in optimizing the EMI SE of composites.

In this study, we used two types of 2D materials as fillers: $Ti_3C_2T_x$ MXene and boron nitride nanosheets (BNNSs). MXene, an emerging 2D material for EMI shielding, is the general name of transition metal carbides/carbonitrides and has the general formula of $M_{n+1}X_nT_x$, where M is an early transition metal (e.g., Ti, Zr, V, Nb, Ta, and Mo) and X is C or N. T_x represents functional groups such as -O, -F, or -OH [11]. In the MXene family, the most studied $Ti_3C_2T_x$ has a high specific surface area, high electrical conductivity, and abundant functional groups [12-15]. These groups make MXene polar, making it hydrophilic and allowing it to disperse in water without a dispersant, thus making it easy to react with other materials. Despite these excellent properties of MXene, it is known to oxidize easily, which is a significant obstacle for practical use. This deteriorates MXene's performance over time, dramatically reducing the EMI shielding effect. BNNSs, another type of 2D materials, have gained prominence as thermally conductive fillers due to their high thermal conductivity, electrically insulation properties, high thermal stability, and chemical resistance [16, 17]. Notably, BNNSs possess the quality of being oxidation-resistant and inert to most chemical reactions, which can delay the oxidation of MXene [18, 19]. Therefore, we expected the synergistic effects between MXene and BNNSs to enhance EMI SE and oxidation stability.

To realize durable and outstanding EMI SE, we proposed polystyrene (PS)@MXene@BNNSs microspheres and then fabricated the composite with a 3D structured filler network using the hot-pressing method. To prepare PS@MXene@BNNSs microspheres like the core-double-shell structure, we introduced electrostatic force by fabricating positive-charged PS, negative-charged MXene via various functional groups, and positive-charged BNNSs by surface modification. After constructing the 3D filler networks through hot pressing, the composite with the 3D continuous networks exhibited excellent EMI SE.

2. MATERIALS AND METHODS

2.1. Synthesis of Polystyrene (PS)

PS was synthesized through the dispersion polymerization reaction of styrene monomer (Duksan). Dispersion polymerization is a type of precipitation polymerization where the

monomer and initiator are entirely dispersed [20, 21]. However, as polymerization progresses and the molecular weight of the polymer exceeds a certain level, it does not disperse and precipitate. First, the styrene monomer was reacted with activated alumina (Daejung Chemical) for activation. To prepare PS with a positive surface charge, 4 ml of purified styrene monomer, 215.9 mg of polyvinyl pyrrolidone (Daejung), 18.9 mg of 2,2-azobisisobutyronitrile (99%, Daejung), and 0.1 ml of [2-(methacryloyloxy)ethyl]trimethylammonium chloride solution (DMC, 75 wt.%, Sigma-Aldrich) were dispersed in a three-necked flask containing 40 ml of ethanol and 4 ml of deionized (DI) water. DMC provided a positive functional group on the PS surface, making the surface charge of the entire molecule positive. This solution was reacted at 70 degrees for 30 min while purging with nitrogen and then stirred at 500 rpm for 18 h while continuously supplying nitrogen. The resulting solution was washed thrice with ethanol using a centrifuge. Finally, it was dried under vacuum at 50 degrees for 24 h to obtain PS with a positive charge.

2.2. Synthesis of $Ti_3C_2T_x$ MXene Nanosheets

$Ti_3C_2T_x$ MXene can be obtained by selectively etching the Al layers of titanium aluminum carbide (Ti_3AlC_2 MAX, >90%, <40 µm particle size, Sigma-Aldrich). For etching, acidic solutions of fluorides, such as hydrofluoric acid [22], ammonium hydrogen bifluoride [23], or a solution mixed with hydrochloric acid (HCl) and lithium fluoride (LiF) [24], are used. Among these, the HCl and LiF method provides a high yield, is safe, and can be synthesized quickly and easily. 4.8 g of LiF (Fujifilm) and 60 ml of 9 M HCl were added into a Teflon container and stirred until LiF was completely dissolved. The temperature of the solution was raised to 35 degrees, and 3 g of Ti_3AlC_2 was slowly added. Then, the mixture was reacted at 350 rpm for 24 h. The reacted solution was repeatedly centrifuged at 8000 rpm for 10 min using DI water until the pH was about 6. When the pH of the supernatant reached about 6, unreacted substances and impurities were removed, and single-layer or few-layer $Ti_3C_2T_x$ MXene was obtained by centrifuging at 1000 g for 20 min. The supernatant that did not settle was filtered using a vacuum-assisted filtration device with cellulose ester membrane filter (MCE, pore size: 20 µm, Hyundai micro) and dried at room temperature under vacuum for 36 h. The dried MXene was mixed with DI water to attain a concentration of 1 mg/ml. The mixed solution was purged with Ar gas (99.99% of purity) for over 30 min. Subsequently, while continuously supplying Ar, it was put into an ultra-sonicator filled with ice and ultrasonically treated. Consequently, the Al layers were removed, and each layer of the layered structure of MXene was exfoliated. MXene nanosheets with a negative surface charge were thus obtained.

2.3. Synthesis of Boron Nitride Nanosheets (BNNSs)

1.5 g of bulk hexagonal-boron nitride (h-BN, 98%, Sigma-Aldrich) was put into a solution mixed with 150 ml of DI water and 150 ml of isopropanol (IPA, 99.8%, Samchun Pure Chemicals) and ultrasonically treated for 12 h. h-BN exists in a hexagonal columnar layered structure. After ultrasonication, each layer was exfoliated to obtain thin layers of BNNSs. After ultrasonic treatment, it was centrifuged at 2000 rpm for 20 min, and the supernatant that did not settle was vacuum-assisted filtered using an MCE filter to obtain sufficiently exfoliated BNNSs. The filtered BNNSs were dried at a temperature of 100 degrees for 10 h. The surface of the obtained BNNSs had a -OH functional group, which was formed when each layer was separated, thus lending it a negative surface charge. To

change this to a positive charge, it was reacted with (3-Aminopropyl)triethoxysilane (APTES, 99 %, Sigma-Aldrich). APTES reacted with the -OH on the surface of BNNSs, and the -NH$_2$ functional group at the end changed the surface charge to positive [25]. 0.015 g of APTES was put into 25 ml of ethanol and reacted at 60 degrees for 30 min. Then, 0.5 g of BNNSs was added and stirred at 80 degrees for 6 h. After the reaction, it was washed three times with ethanol to remove impurities. Finally, it was dried at 100 degrees for 12 h to obtain BNNSs-APTES with a positive surface charge.

2.4. Fabrication of Polystyrene@MXene@Boron Nitride Composite

PS has a positive charge and MXene has a negative charge; therefore, when the two materials react, they attract each other due to electrostatic forces. Moreover, PS has a spherical 3D structure and MXene has a planar 2D structure, so MXene can stick to PS like a shell, resulting in a core-shell structure of PS@MXene. If a sufficient amount of MXene reacts with PS, MXene covers the surface of PS, giving it a negative surface charge. When these PS@MXene particles with a negative charge react with BNNSs-APTES with a positive charge, the same electrostatic forces work to obtain PS@MXene@BNNSs microspheres with a double-core-shell structure.

We prepared a solution of PS dispersed in DI water at 3 mg/ml and a solution of BNNSs-APTES dispersed in DI water at 5 mg/ml. The previously prepared MXene solution was slowly added to the PS solution at 33.3 ml with varying amounts (3, 5, 7, 10, 13, 15 wt%) and then stirred at 500 rpm for 2 h. At this stage, PS@MXene microspheres were formed, and various MXene concentrations were tested to determine the sufficient amount that could react with BNNSs-APTES. Subsequently, an amount of BNNSs-APTES solution, equal to the amount of the MXene solution, was slowly added and reacted at 500 rpm for 2 h. After the reaction, the particles and DI water were separated using vacuum filtration with an MCE filter. When dried at 50 degrees for 12 h, PS@MXene@BNNSs microspheres were obtained. A composite with a 3D structure of filler network was obtained by adding 0.1 g of PS@MXene@BNNSs microspheres into a mold for hot pressing and pressing at a temperature of 130 degrees with a pressure of 10 MPa for 30 min.

2.5. Characterization

The zeta potential was measured with a particle size and zeta potential analyzer (Delsa Nano C particle analyzer, Beckman Coulter) to determine the change in charge on the material surface. X-ray photoelectron spectroscopy (XPS, K-alpha+, ThermoFisher Scientific) was used to confirm whether each material was synthesized, and surface modification was performed correctly. A particle size analyzer (PSA; S3500, Microtrac) was used to confirm whether the polymerization of PS occurred uniformly. Field-emission scanning electron microscopy (FE-SEM; SIGMA 300, Carl Zeiss) was used to analyze the surface morphologies of all the materials. Additionally, X-ray diffraction (XRD; New D8-advance, Bruker-AXS) was utilized to analyze the MXene and confirm whether the Al layer in the Ti$_3$AlC$_2$ MAX phase was completely etched. Fourier-transform infrared spectrometer (FT-IR; Nicolet 6700, Thermo Scientific) was used to determine whether APTES worked adequately on the surface of BNNSs, and the EMI SE was measured using a vector network analyzer (VNA; 8720D, Hewlett-Packard, Palo Alto, USA).

3. RESULTS AND DISCUSSION

Fig. 1 illustrates the fabrication process of the PS@MXene@BNNSs composite. Dispersion polymerization was used to synthesize PS, incorporating an initiator, monomer, and the positive agent DMC to create PS with a positive surface charge. MXene initially exists in the MAX phase, where MX layers alternate with A layers. By etching the Al layers with a LiF/HCl solution, layered MXene was obtained. Delaminating these layers produced MXene flakes. BN typically exists in a bulk layered structure, but BNNSs was produced by exfoliating BN with DI water and IPA. These BNNSs contain -OH groups, which reacted with APTES to yield silanized BNNSs-APTES. Using self-assembly driven by surface charges, the materials were sequentially assembled as MXene and BNNSs-APTES onto the PS microspheres, forming PS@MXene@BNNSs microspheres. Finally, hot pressing these microspheres resulted in the PS@MXene@BNNSs composite.
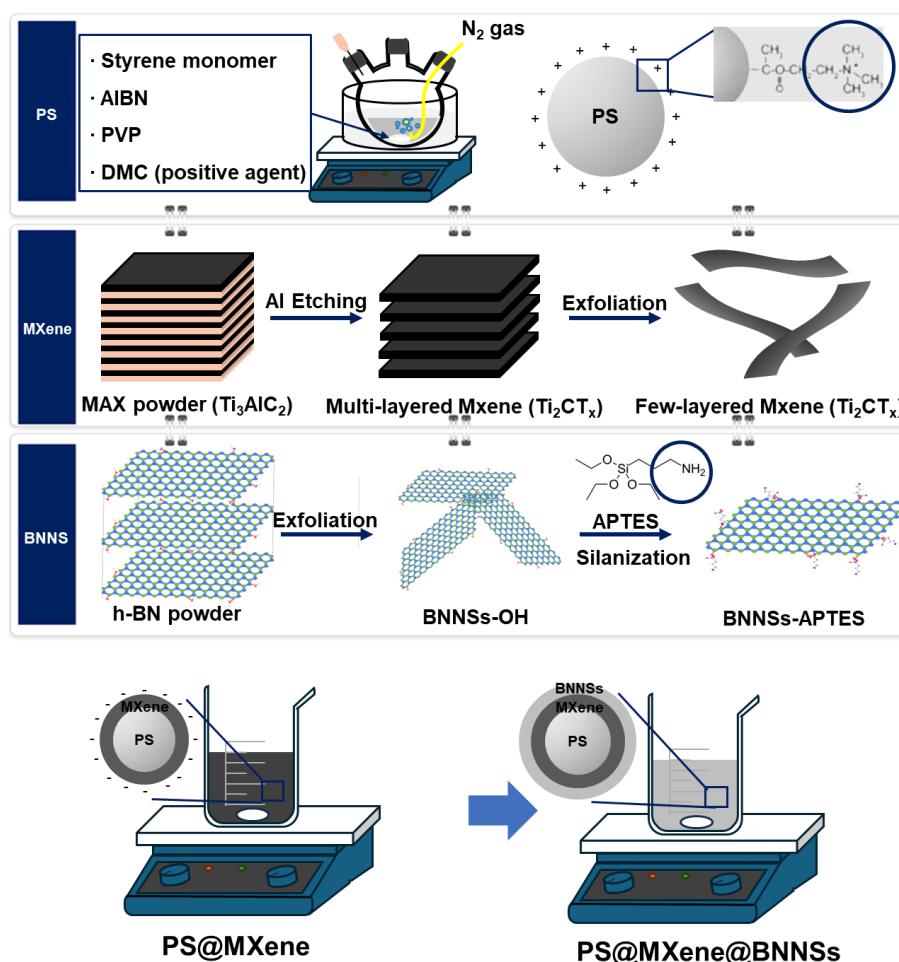

Fig. 1 Schematic illustration of the fabrication of PS@MXene@BNNSs

During synthesizing PS, DMC was added to change the PS surface so that it could be positively charged. The functional group -N(CH$_3$)$_3^+$ in DMC imparted a positive surface charge, which was confirmed through XPS analysis and zeta potential measurements. Fig. 2(a) compares the zeta potential values of the normal PS without DMC and the charged PS with DMC. The zeta potential represents the potential at the slipping plane of a particle [26]. When charged particles are dispersed in a solution, counterions in the solution adsorb onto the particle to neutralize the particle's charge, forming an electrical double layer. This double layer comprises a stern layer and a diffuse charge layer. The slipping plane is defined as the outer boundary where the particles move, and the potential at this plane is known as the zeta potential, indicating the electrical properties of the interface. Normal PS showed a negative zeta potential (-22.94 mV), but with the addition of DMC, the charged PS exhibited a positive zeta potential (26.5 mV), confirming the effective functionalization of PS with DMC. Fig. 2(b) displays the XPS results for the N 1s region of the charged PS. The peak intensity of around 403 eV corresponds to the -N(CH$_3$)$_3^+$ functional group, which is the terminal part of DMC, confirming the presence of DMC on the PS surface.

PSA and FE-SEM analyses were performed to verify the uniform particle size of the synthesized PS via dispersion polymerization. Fig. 2(c) shows the particle size distribution of the charged PS measured by PSA, indicating that most particles were around 0.7 µm in size, with a D50 value of 0.741 µm. Fig. 2(d) provides an FE-SEM image, revealing uniformly sized spherical PS particles with smooth surfaces.
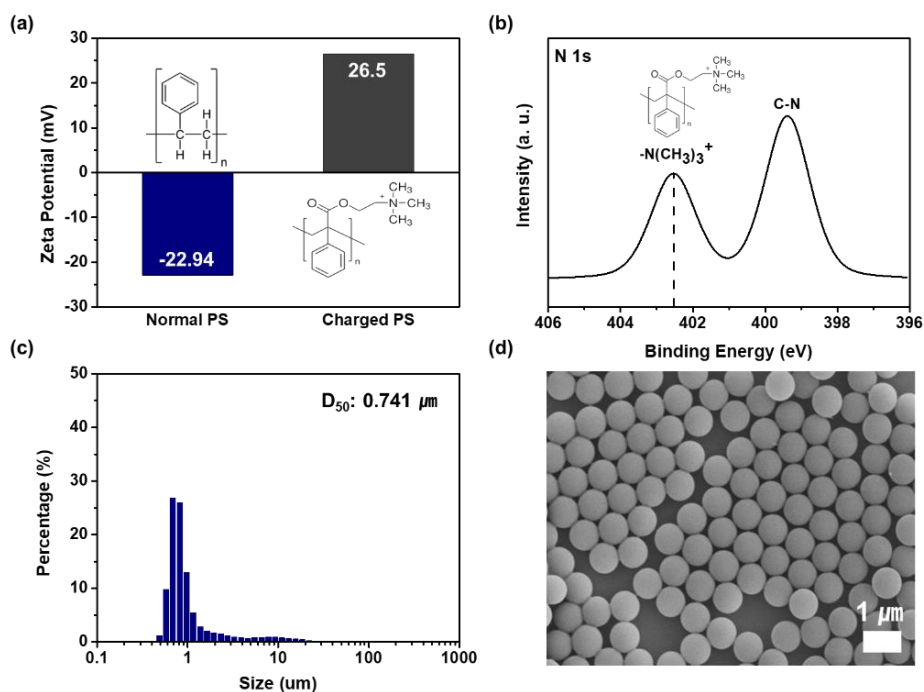

Fig. 2 Characterization of the positively charged polystyrene particles: (a) zeta potential measurements, (b) XPS analysis, (c) particle size distribution profile, and (d) FE-SEM image

When the MAX phase transformed into the MXene phase, the existing Al layers were removed, and various functional groups formed, which altered the surface characteristics. These functional groups, such as -OH and -F, carried negative charges, resulting in the etched MXene having a negatively charged surface. Fig. 3(a) shows the zeta potential of MXene, measured at -52.26 mV, indicating a negative surface charge. Additionally, the zeta potential provides insights into dispersibility, suggesting that MXene has good dispersion stability in water. Fig. 3(b) and 3(c) demonstrate the successful etching from the MAX phase to the MXene phase. Figure 3(b) presents the MAX and MXene XPS analysis. The disappearance of the Al peak after transformation to MXene confirms that Al was entirely etched away by the acidic solution. The structural change from MAX to MXene is evident in the XRD patterns (Figure 3(c)). As the transformation progressed, the Al layers were removed by LiF/HCl, causing the characteristic peaks at (101), (103), (104), and (105) to disappear [27]. The broadening of the (002) peak was also observed, which can be attributed to the increased interlayer distance after Al removal. The etched MXene exhibited an accordion-like layered structure, which was delaminated through simple sonication. This delaminated MXene was very thin and flexible, as shown in Figure 3(d).
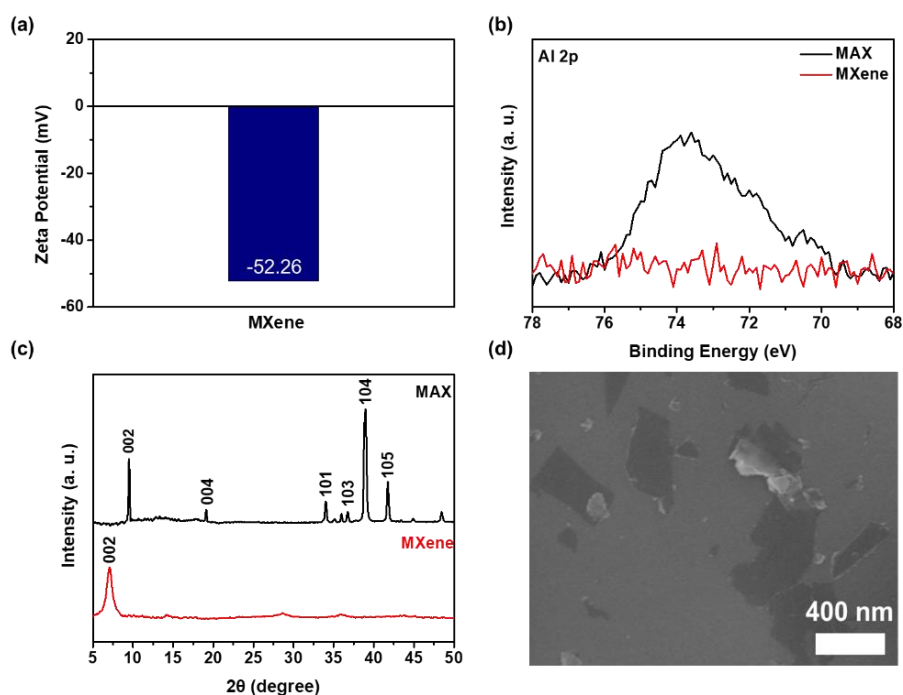

Fig. 3 Characterization of $Ti_3C_2T_x$ MXene and Ti_3AlC_2 MAX: (a) zeta potential measurements, (b) XPS analysis, (c) XRD analysis, and (d) FE-SEM image

The layered structure of BN transitioned to BNNSs as the interlayer bonds broke during sonication in a mixture of IPA and DI water. During this process, -OH functional groups formed on the surface of BNNSs, imparting a negative charge. To facilitate interaction with PS@MXene, which also had a negative charge, it was necessary to change the surface

charge to positive. This was achieved by reacting the -OH groups with APTES. Figure 4(a) shows the zeta potential measurements of BNNSs and BNNSs-APTES. BNNSs had a value of -36.7 mV, which changed to +37.1 mV after reacting with APTES, indicating that the -NH_2^+ groups of APTES effectively modified the surface of BNNSs to a positive charge. Figures 4(b) and 4(c) present the XPS and FT-IR results of BNNSs and BNNSs-APTES, respectively. Since BNNSs consist of boron and nitrogen, no Si peak was observed. The XPS results show that Si, present in APTES, was detectable in BNNSs-APTES. Additionally, the FT-IR results reveal a -CH_2-related peak, which was absent in BNNSs but appeared in BNNSs-APTES, further confirming the presence of APTES on the BNNSs surface [28, 29]. This demonstrates that APTES effectively reacted with the surface of BNNSs, converting the surface charge from negative to positive. The FE-SEM image (Fig. 4(d)) also shows the well-exfoliated appearance of BNNSs-APTES, confirming successful exfoliation.
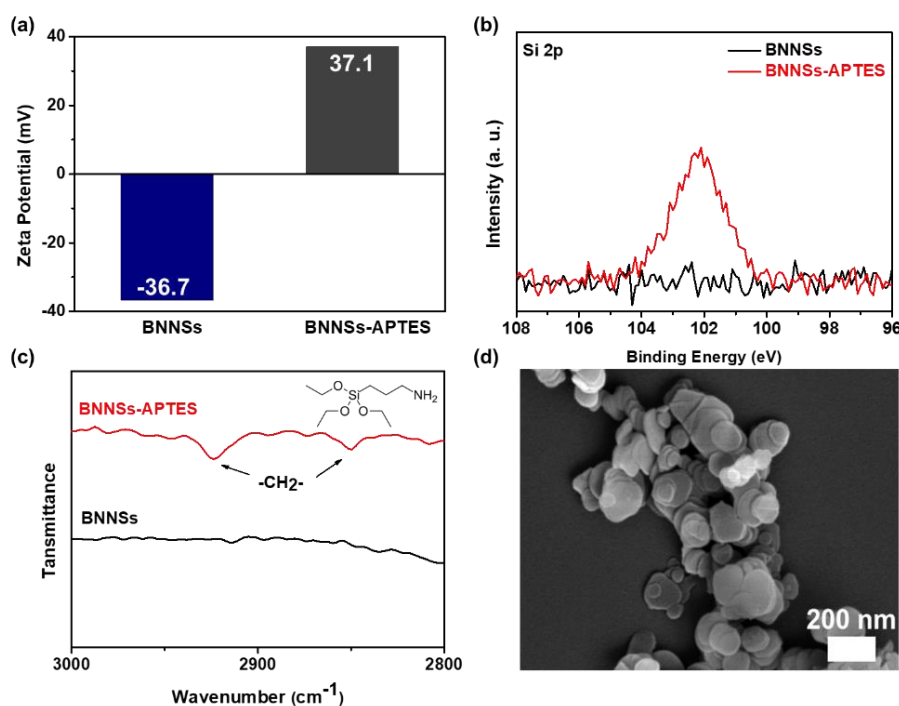

Fig. 4 Characterization of boron nitride nanosheets (BNNSs) and BNNSs-APTES: (a) zeta potential measurements, (b) XPS analysis, (c) FT-IR analysis, and (d) FE-SEM image

In this study, the surface charge of materials was adjusted through surface modification for use in the self-assembly method. The adjusted surface charge was confirmed by zeta potential measurements, as shown in Fig. 5(a). The zeta potential of PS was measured at +26.5 mV, while MXene exhibited a negative charge of -52.26 mV. BNNSs-APTES had a positive charge of +37.1 mV. These surface charges facilitated the subsequent reactions. Initially, PS and MXene were reacted together, with sufficient MXene added to ensure a

significant negative charge for further reaction with BNNSs-APTES. The zeta potential of PS@MXene, depending on the MXene concentration, is depicted in Fig. 5(b). The zeta potential gradually decreased with an increase in the MXene content, indicating the effect of MXene on the particle surface. The zeta potential saturated around 10 wt% MXene. PS@MXene containing 10 wt% MXene was then used for further modification. The morphology of PS@MXene with 10 wt% MXene is shown in Fig. 5(c). The image reveals that the smooth surface of PS was uniformly covered by thin MXene flakes, resulting in a negative surface charge. After reacting with BNNSs-APTES, the morphology is shown in Fig. 5(d). BNNSs-APTES was added at five times the amount of MXene to ensure complete coverage of PS@MXene. The final microspheres, PS@MXene@BNNSs-APTES, show BNNSs-APTES uniformly covering the negative-charged PS@MXene particles. These results demonstrate that surface charge modification enabled straightforward coating processes using surface charge-driven reactions. This approach offers a simple and effective method for coating materials through self-assembly.
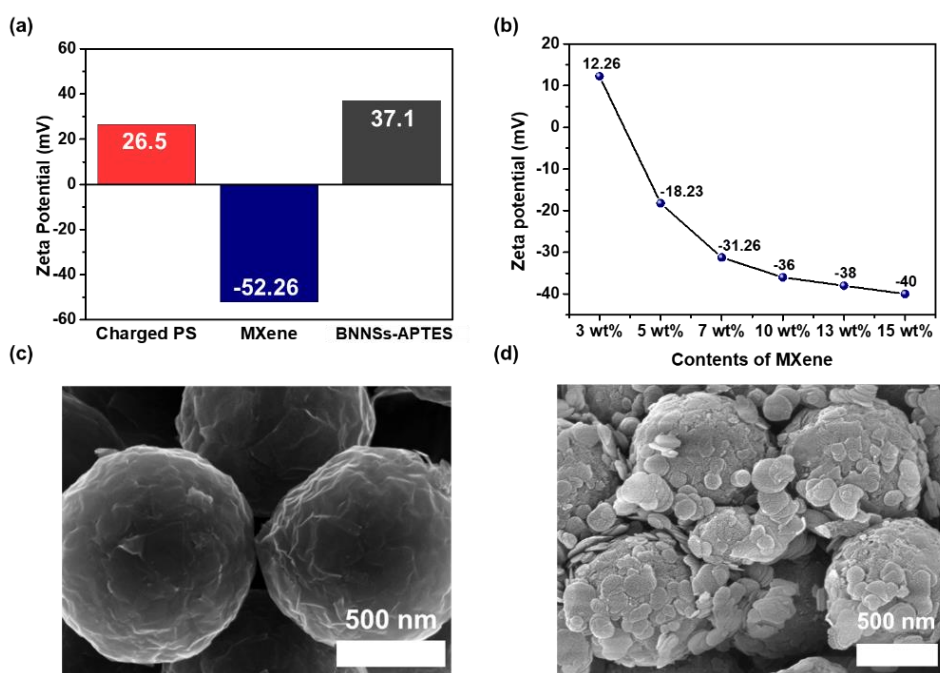

Fig. 5 (a) Zeta potential of the charged PS, $Ti_3C_2T_x$ MXene, and BNNSs-APTES; (b) zeta potential of PS@MXene as contents of MXene; (c) FE-SEM image of PS@MXene; and (d) FE-SEM image of PS@MXene@BNNSs-APTES

The initial electromagnetic wave undergoes intensity modulation through various mechanisms when it encounters the surface and interior of a shield. This phenomenon arises due to the impedance and refractive index difference between the air and the shield material. As these electromagnetic waves pass through the shield, they are attenuated, leading to a decrease in intensity. The impedance difference on the shield's front and back

surfaces induces the reflection of electromagnetic waves. The degree to which the shield blocks and reduces the initial electromagnetic wave is defined as EMI SE (SE_T), which is expressed in logarithmic scale units and represents the reduction in intensity of the transmitted electromagnetic wave compared to the initial wave. It is defined as follows:

$$SE_T \ (dB) \ = \ 10 \ log \frac{P_T}{P_0} \ = \ 20 \ log \frac{E_T}{E_0} \tag{1}$$

where P_0 and E_0 are the initial power density and electric field strength, respectively, and P_T and E_T represent those of the transmitted electromagnetic waves. According to the Schelkunoff formula[30], the EMI SE occurs through three mechanisms: absorption loss (SE_A), reflection loss (SE_R), and multiple reflection loss (SE_M) [31].

$$SE_T \ = \ SE_A \ + \ SE_R \ + \ SE_M \tag{2}$$

As the initial electromagnetic wave passes through the shield, it is absorbed according to the attenuation constant α. The strength of the initial electromagnetic wave decreases exponentially with the shield thickness d, according to α, and is represented through the following formula:

$$E \ = \ E_0 e^{-\alpha d} \tag{3}$$

The attenuation constant α is defined as follows:

$$\alpha \ = \ \omega \sqrt{\frac{\mu \varepsilon}{2} \sqrt{1 + (\frac{\sigma}{\omega \varepsilon})^2} \ - \ 1} \tag{4}$$

where ω is the angular frequency, μ is the magnetic permeability, ε is the dielectric permittivity, and σ is the electrical conductivity. For effective absorption loss of electromagnetic waves, the shield must possess a high electrical conductivity, large dielectric permittivity, or high magnetic permeability. Most of the absorbed electromagnetic waves are converted into thermal energy. The absorption loss SE_A is defined by the skin depth δ and the shield thickness d as follows [32]:

$$SE_A(dB) \ = \ 20 \ log \, e^{\alpha d} \ = \ 20 \left(\frac{d}{\delta}\right) \log_{10} e \tag{5}$$

Skin depth δ is the distance through which the wave decreases to e^{-1} of the original incident wave intensity.

Reflection loss (SE_R) occurs at the shield's surface due to the impedance or refractive index difference between the air and the shield material. This loss can be expressed by the Fresnel equation, which involves electric conductivity σ, frequency of the electromagnetic wave f, and magnetic permeability μ.

$$SE_R \ (dB) \ = \ 20 \ log \frac{(\eta+\eta_0)^2}{4\eta\eta_0} = \ 39.5 \ + \ 10 \ log \frac{\sigma}{2\pi f \mu} \tag{6}$$

where η and η_0 represent the impedances of the shield and air, respectively. Reflection loss is influenced by the impedance difference, electrical conductivity of the shield, magnetic permeability, and the frequency of the incident electromagnetic waves.

Multiple reflection loss is significantly affected by the shield thickness. The electromagnetic wave reflected from the shield's back surface may encounter the front surface again, causing further reflections. The electromagnetic wave intensity decreases

progressively as these reflections continue between the front and back surfaces. Multiple reflection loss can be expressed as follows:

$$SE_M \;=\; 20\log_{10}(1 - e^{-2\alpha d}) \;=\; 20\,\log_{10}\left(1 - e^{-\frac{2d}{\delta}}\right) \tag{7}$$

Multiple reflection loss becomes negligible if the total EMI SE exceeds 15 dB or if the shield thickness is similar to or greater than the skin depth.

The total EMI SE can be calculated from the scattering parameters obtained from two ports using a VNA. S_{11} represents the ratio of the voltage input to port 1 and the voltage output from port 1, and S_{21} represents the ratio of the voltage input to port 1 and the voltage output from port 2. Similarly, S_{22} and S_{12} represent the reflection and transmission parameters for port 2, respectively. For a uniform shield, $S_{11} = S_{22}$ and $S_{21} = S_{12}$. SE_A and SE_R can be defined in terms of these scattering parameters as follows [33]:

$$T \;=\; |S_{21}|^2 \tag{8}$$

$$R \;=\; |S_{11}|^2 \tag{9}$$

$$1 \;=\; A + R + T \tag{10}$$

$$SE_A \;=\; -10\log_{10}\frac{T}{1-R} \tag{11}$$

$$SE_R \;=\; -10\log_{10}(1 - R) \tag{12}$$

Here, A, R, and T represent the absorption, reflection, and transmission power coefficients, respectively.

The total EMI SE measured by VNA for PS@MXene and PS@MXene@BNNSs is shown in Fig. 6. The composites were fabricated through hot pressing, and the EMI SE of these composites was compared based on the coating of BNNSs-APTES. It was observed that in all the frequency ranges, the presence of BNNSs significantly enhanced the performance.
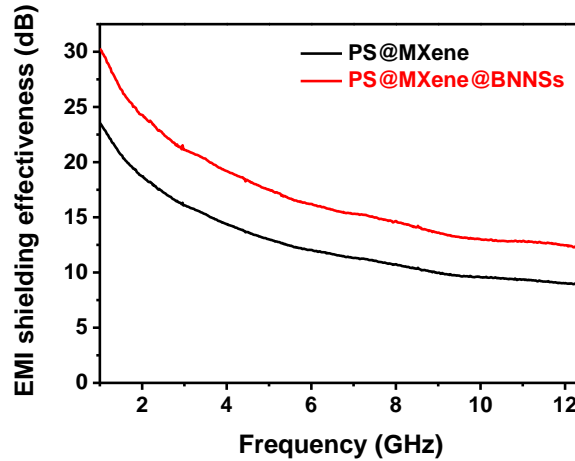

Fig. 6 EMI SE of PS@MXene and PS@MXene@BNNSs

This improvement can be attributed to the BNNSs layer encapsulating the oxidizing MXene, thereby preventing its oxidation. Additionally, the repeated interfaces of various materials increased the EMI SE due to the impedance difference between each material. As seen in the initial part of the graph, the composites exhibited relatively high EMI SE. Considering that a shielding effectiveness of 20 dB or higher corresponds to 99% blockage of electromagnetic waves, the composites developed in this study demonstrated commendable performance, particularly in the low-frequency range. Furthermore, the thicknesses of the fabricated composites were relatively thin, at just 0.8 mm. Since the thickness of the composite greatly influences EMI SE, the performance observed in this study can be considered excellent.

4. CONCLUSIONS

In this study, we fabricated a multifunctional composite with electromagnetic wave shielding capabilities by controlling the surface charge of PS, MXene, and BNNSs. It is crucial to control the surface charge of each material precisely to achieve an optimal composite. Since MXene and BNNSs need to bind to the surface of spherical PS particles, it is important to form a nanosheet of the 2D material. For PS, the surface was initially negatively charged after dispersion polymerization, but it became positively charged with the addition of DMC. This allowed us to create PS@MXene microspheres by reacting the positively charged PS with negatively charged MXene. Similarly, we modified BNNS (with a negative surface charge) with APTES to impart a positive charge, enabling the fabrication of PS@MXene@BNNSs microspheres through a self-assembly reaction. These microspheres were then hot-pressed to form the PS@MXene@BNNSs composite.

The PS@MXene@BNNSs composite exhibited excellent electromagnetic wave shielding efficiency in the low-frequency range. Furthermore, it consistently demonstrated higher shielding efficiency than the PS@MXene composite, indicating the oxidation prevention effect of BNNS. Given that BNNSs have excellent thermal conductivity and completely encapsulate PS, the resulting PS@MXene@BNNSs composite is also expected to possess high thermal conductivity.

Therefore, the PS@MXene@BNNSs composite developed in this study shows significant potential for use in electronic devices requiring electromagnetic wave shielding. It is particularly suitable for applications where insulation, low-frequency electromagnetic wave generation, and thin material thickness are essential. Additionally, the method proposed in this study offers a solution for both thermal management and electromagnetic wave shielding, providing a practical approach for manufacturing a dual conduction path (thermal and electrical conduction).

REFERENCES

1. Shahzad, F., Alhabeb, M., Hatter, C.B., Anasori, B., Man Hong, S., Koo, C.M., Gogotsi, Y., 2016, *Electromagnetic interference shielding with 2D transition metal carbides (MXenes)*, Science, 353(6304), pp. 1137-1140.
2. Li, N., Huang, Y., Du, F., He, X., Lin, X., Gao, H., Ma, Y., Li, F., Chen, Y., Eklund, P.C., 2006, *Electromagnetic interference (EMI) shielding of single-walled carbon nanotube epoxy composites*, Nano letters, 6(6), pp. 1141-1145.
3. Al-Saleh, M.H., Saadeh, W.H., Sundararaj, U., 2013, *EMI shielding effectiveness of carbon based nanostructured polymeric materials: a comparative study*, Carbon, 60, pp. 146-156.
4. Ha, H., Qaiser, N., Yun, T.G., Cheong, J.Y., Lim, S., Hwang, B., 2023, *Sensing mechanism and application of mechanical strain sensor: a mini-review,* Facta Universitatis-Series Mechanical Engineering, 21(4), pp. 751-772.
5. Kim, H., Qaiser, N., Hwang, B., 2023, *Electro-mechanical response of stretchable pdms composites with a hybrid filler system*, Facta Universitatis-Series Mechanical Engineering, 21(1), pp. 051-061.
6. Choi, C., Ashby, D.S., Butts, D.M., DeBlock, R.H., Wei, Q., Lau, J., Dunn, B., 2020, *Achieving high energy density and high power density with pseudocapacitive materials*, Nature Reviews Materials, 5(1), pp. 5-19.
7. Asmatulu, R., Bollavaram, P.K., Patlolla, V.R., Alarifi, I.M., Khan, W.S., 2020, *Investigating the effects of metallic submicron and nanofilms on fiber-reinforced composites for lightning strike protection and EMI shielding*, Advanced Composites and Hybrid Materials, 3, pp. 66-83.
8. Bayat, A., Ebrahimi, M., Ardekani, S.R., Iranizad, E.S., Moshfegh, A.Z., 2021, *Extended Gibbs free energy and laplace pressure of ordered hexagonal close-packed spherical particles: A wettability study*, Langmuir, 37(28), pp. 8382-8392.
9. Choi, C., Lim, S., Yun, T.G., Marinkovic, D., Matteini, P., Hwang, B., 2024, *Ag nanowire-based conductive textiles for electronic devices: an introductory review*, Nano, doi: 10.1142/S1793292024300123
10. Thomassin, J.-M., Jérôme, C., Pardoen, T., Bailly, C., Huynen, I., Detrembleur, C., 2013*, Polymer/carbon based composites as electromagnetic interference (EMI) shielding materials*, Materials Science and Engineering: R: Reports, 74(7), pp. 211-232.
11. Naguib, M., Mochalin, V.N., Barsoum, M.W., Gogotsi, Y., 2014, *25th anniversary article: MXenes: a new family of two-dimensional materials*, Advanced materials, 26(7), pp. 992-1005.
12. Qi, F., Wang, L., Zhang, Y., Ma, Z., Qiu, H., Gu, J., 2021, *Robust $Ti_3C_2T_x$ MXene/starch derived carbon foam composites for superior EMI shielding and thermal insulation*, Materials Today Physics, 21, 100512.
13. Wang, L., Qiu, H., Song, P., Zhang, Y., Lu, Y., Liang, C., Kong, J., Chen, L., Gu, J., 2019, *3D Ti3C2Tx MXene/C hybrid foam/epoxy nanocomposites with superior electromagnetic interference shielding performances and robust mechanical properties*, Composites Part A: Applied Science and Manufacturing, 123, pp. 293-300.
14. Wang, L., Chen, L., Song, P., Liang, C., Lu, Y., Qiu, H., Zhang, Y., Kong, J., Gu, J., 2019, *Fabrication on the annealed $Ti_3C_2T_x$ MXene/Epoxy nanocomposites for electromagnetic interference shielding application*, Composites Part B: Engineering, 171, pp. 111-118.
15. Verma, R., Thakur, P., Chauhan, A., Jasrotia, R., Thakur, A., 2023, *A review on MXene and its' composites for electromagnetic interference (EMI) shielding applications*, Carbon, 208, pp. 170-190.
16. Boldrin, L., Scarpa, F., Chowdhury, R., Adhikari, S., 2011, *Effective mechanical properties of hexagonal boron nitride nanosheets*, Nanotechnology, 22(50), 505702.
17. Weng, Q., Kvashnin, D.G., Wang, X., Cretu, O., Yang, Y., Zhou, M., Zhang, C., Tang, D.M., Sorokin, P.B., Bando, Y., 2017, *Tuning of the optical, electronic, and magnetic properties of boron nitride nanosheets with oxygen doping and functionalization*, Advanced materials, 29(28), 1700695.
18. Biscarat, J., Bechelany, M., Pochat-Bohatier, C., Miele, P., 2015, *Graphene-like BN/gelatin nanobiocomposites for gas barrier applications*, Nanoscale, 7(2), pp. 613-618.
19. Meziani, M.J., Song, W.L., Wang, P., Lu, F., Hou, Z., Anderson, A., Maimaiti, H., Sun, Y.P., 2015, *Boron nitride nanomaterials for thermal management applications*, ChemPhysChem, 16(7), pp. 1339-1346.
20. Kawaguchi, S., Ito, K., 2005, *Dispersion polymerization*, Polymer Particles, 175, pp. 299-328.
21. Arshady, R., 1992, *Suspension, emulsion, and dispersion polymerization: A methodological survey*, Colloid and polymer science, 270, pp. 717-732.
22. Chu, Y.Z., Hoover, M., Ward, P., Lau, K.C., 2024, *First-principles study of MXene properties with varying hydrofluoric acid concentration*, Iscience, 27(2), 108784.
23. Pahlevaninezhad, M., Sadri, R., Momodu, D., Eisawi, K., Pahlevani, M., Naguib, M., Roberts, E.P., 2024, *Ammonium Bifluoride-Etched MXene Modified Electrode for the All− Vanadium Redox Flow Battery*, Batteries & Supercaps, 7(4), e202300473.
24. Zhang, T., Pan, L., Tang, H., Du, F., Guo, Y., Qiu, T., Yang, J., 2017, *Synthesis of two-dimensional $Ti_3C_2T_x$ MXene using HCl+ LiF etchant: enhanced exfoliation and delamination*, Journal of Alloys and Compounds, 695, pp. 818-826.

25. Acres, R.G., Ellis, A.V., Alvino, J., Lenahan, C.E., Khodakov, D.A., Metha, G.F., Andersson, G.G., 2012, *Molecular structure of 3-aminopropyltriethoxysilane layers formed on silanol-terminated silicon surfaces*, The Journal of Physical Chemistry C, 116(10), pp. 6289-6297.

26. Clogston, J.D., Patri, A.K., 2011, *Zeta potential measurement, Characterization of nanoparticles intended for drug delivery*, 697, pp. 63-70.

27. Luo, J., Tao, X., Zhang, J., Xia, Y., Huang, H., Zhang, L., Gan, Y., Liang, C., Zhang, W., 2016, *Sn4+ ion decorated highly conductive Ti3C2 MXene: promising lithium-ion anodes with enhanced volumetric capacity and cyclic performance*, ACS nano, 10(2), pp. 2491-2499.

28. Hou, J., Li, G., Yang, N., Qin, L., Grami, M.E., Zhang, Q., Wang, N., Qu, X., 2014, *Preparation and characterization of surface modified boron nitride epoxy composites with enhanced thermal conductivity*, Rsc Advances, 4(83), pp. 44282-44290.

29. Oh, H., Kim, J., 2019, *Fabrication of polymethyl methacrylate composites with silanized boron nitride by in-situ polymerization for high thermal conductivity*, Composites Science and Technology, 172, pp. 153-162.

30. Schulz, R.B., Plantz, V., Brush, D., 1988, *Shielding theory and practice*, IEEE Transactions on electromagnetic compatibility, 30(3), pp. 187-201.

31. Joshi, A., Datar, S., 2015, *Carbon nanostructure composite for electromagnetic interference shielding*, Pramana, 84, pp. 1099-1116.

32. Iqbal, A., Sambyal, P., Koo, C.M., 2020, *2D MXenes for electromagnetic shielding: a review*, Advanced Functional Materials, 30(47), 2000883.

33. Xu, Y., Yang, Y., Yan, D.-X., Duan, H., Zhao, G., Liu, Y., 2019, *Flexible and conductive polyurethane composites for electromagnetic shielding and printable circuit*, Chemical Engineering Journal, 360, pp. 1427-1436.